The Isolated Sixth Gelsolin Repeat and Headpiece Domain of Villin Bundle F-Actin in the Presence of Calcium and Are Linked by a 40-Residue Unstructured Sequence[†,‡]

Serge L. Smirnov,[§] Nancy G. Isern,[||] Zhenghui G. Jiang,[§] David W. Hoyt,[||] and C. James McKnight*[,§]

Department of Physiology and Biophysics, Boston University School of Medicine, 715 Albany Street, Boston, Massachusetts 02118, and WR Wiley Environmental Molecular Sciences Laboratory, High Field NMR Facility, P.O. Box 999, K8-98 Richland, Washington 99352

Received January 18, 2007; Revised Manuscript Received May 1, 2007

ABSTRACT: Villin is an F-actin regulating, modular protein with a gelsolin-like core and a distinct C-terminal "headpiece" domain. Localized in the microvilli of the absorptive epithelium, villin can bundle F-actin and, at higher calcium concentrations, is capable of a gelsolin-like F-actin severing. The headpiece domain can, in isolation, bind F-actin and is crucial for F-actin bundling by villin. While the three-dimensional structure of the isolated headpiece is known, its conformation in the context of attachment to the villin core remains unexplored. Furthermore, the dynamics of the linkage of the headpiece to the core has not been determined. To address these issues, we employ a 208-residue modular fragment of villin, D6-HP, which consists of the sixth gelsolin-like domain of villin (D6) and the headpiece (HP). We demonstrate that this protein fragment requires calcium for structural stability and, surprisingly, is capable of Ca^{2+}-dependent F-actin bundling, suggesting that D6 contains a cryptic F-actin binding site. NMR resonance assignments and ^{15}N relaxation measurements of D6-HP in 5 mM Ca^{2+} demonstrate that D6-HP consists of two independent structural domains (D6 and HP) connected by an unfolded 40-residue linker sequence. The headpiece domain in D6-HP retains its structure and interacts with D6 only through the linker sequence without engaging in other interactions. Chemical shift values indicate essentially the same secondary structure elements for D6 in D6-HP as in the highly homologous gelsolin domain 6. Thus, the headpiece domain of villin is structurally and functionally independent of the core domain.

Villin is a major cytoskeletal protein involved in the upkeep of actin bundles supporting microvilli in the brush-border membrane of the absorptive epithelium cells of the intestine and kidney (*1*). The capacity of villin to organize filamentous actin (F-actin)[1] into tight bundles in vitro and to bind efficiently to F-actin explains its ability to induce microvilli formation in cultured cells (*2*). However, an additional and, perhaps, crucial role of villin may be the catabolism of microvilli after injury (*3*).

A high degree of sequence homology and similar proteolytic cleavage patterns relate villin to gelsolin, an F-actin-severing and -capping predecessor of a number of cytoskeleton-regulating proteins (*1*). The amino acid sequence of villin consists of two distinct parts, the larger N-terminal gelsolin-like "core" and the C-terminal "headpiece" domain (Figure 1). Proteolysis, in vitro, demonstrates that F-actin bundling by villin requires both the core and headpiece domain (*4*).

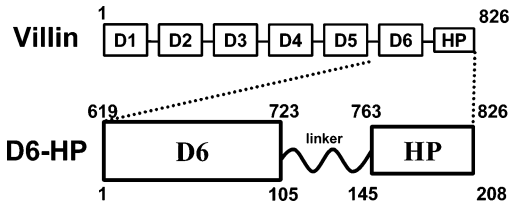

FIGURE 1: Cartoon representation of villin and the 23 kDa D6-HP construct. The villin sequence consists of six gelsolin-like repeats (D1−D6) that compose the gelsolin-like core and the C-terminal headpiece domain (HP). The D6-HP modular villin fragment includes the last gelsolin-like repeat (D6), the linking sequence, and the headpiece (HP). The numbers on top of the D6-HP drawing correspond to the positions in the chicken villin sequence (*1*). Numbers on the bottom specify the same positions in the D6-HP construct and are used by default throughout this work. For the amino acid sequence of D6-HP, see Figure 5.

The sequence of the villin core is ∼50% identical with that of gelsolin and displays the typical gelsolin-like six-fold internal homologous repeat pattern (*5*−*7*). The distinct sequence of the villin headpiece domain is 50% identical to those of other headpiece domains, including those of quail (*8*), supervillin (*9*), and dematin (*10*). The headpiece is unrelated to any other protein sequence in GenBank. Like most other headpiece domains, the 76-residue villin headpiece folds independently into a compact structure and retains its full F-actin binding activity in isolation (*4*, *11*, *12*). In spite of the high level of sequence identity between gelsolin

[†] This work was supported by National Institutes of Health Grant GM062886 to C.J.M.

[‡] The ^1H, ^{15}N, and ^{13}C NMR assignments and R_1, R_2, and heteronuclear NOE values for the D6-HP sample reported here have been deposited in the Biological Magnetic Resonance Data Bank (entry 15097).

* To whom correspondence should be addressed. E-mail: cjmck@bu.edu. Telephone: (617) 638-4042. Fax: (617) 638-4041.

[§] Boston University School of Medicine.

[||] High Field NMR Facility.

[1] Abbreviations: DTT, dithiothreitol; F-actin, filamentous actin; G-actin, monomeric, globular actin; IPTG, isopropyl β-D-1-thiogalactopyranoside; NOE, nuclear Overhauser effect; PIPES, piperazine-1,4-bis(2-ethanesulfonic acid).

10.1021/bi700110v CCC: $37.00
Published on Web 06/05/2007

and the villin core, their domains are not interchangeable. For example, a chimera protein consisting of the three N-terminal villin core domains, three C-terminal gelsolin domains, and the villin headpiece does not induce villin-like F-actin assemblies in vivo (*13*).

Direct structural information about villin is limited to the three-dimensional solution structure of domain 1 (*14*, *15*) and the headpiece domain (*16*) determined by NMR spectroscopy. The structure of domain 1 (14T) is similar to those of other gelsolin-like domains with a five-stranded β-sheet sandwiched between helices (*15*). On the basis of the three-dimensional structure of a villin headpiece construct missing the first nine residues (HP67), we proposed a model for the F-actin binding surface on HP67 (*16*). This model was further refined and corroborated by functional and structural studies (*17*, *18*).

Like many actin remodeling proteins of the gelsolin superfamily, villin is regulated by environmental signals, including calcium. Villin links actin filaments into bundles at physiological levels of Ca^{2+}, whereas it caps and severs F-actin at higher Ca^{2+} concentrations (*1*). Calcium binding sites were proposed to be located in villin core domains 1 (*14*), 4, and 6 (*19*). Interestingly, the C-terminal half of villin, a fragment termed 51T (*20*), binds G-actin in a calcium-dependent fashion. The F-actin binding activity (*11*) and three-dimensional structure of the isolated headpiece are not calcium-dependent.

The crystal structure of villin has not been reported, and no structural data about modular fragments of villin are available. Additionally, no structural data for modular protein fragments containing headpiece domains exist. In contrast to villin, there is a wealth of structural information about gelsolin modular fragments, including the crystal structures of the calcium-free complete protein (*21*) and calcium-bound C-terminal half of gelsolin (*22*). The latter structure clearly shows that gelsolin domains 5 and 6 (G5 and G6, respectively) each have a single calcium ion bound to their surfaces.

Although the isolated villin headpiece domain has been under intense scrutiny, its properties in the context of the core domains still remain untested. Here we present a structural and functional study of D6-HP (Figure 1), the first modular villin fragment containing the headpiece (HP) attached to the sixth core domain (D6). We use heteronuclear NMR spectroscopy to characterize the structure of D6-HP and electron microscopy to assay its F-actin bundling. We utilize this villin fragment to determine whether the headpiece remains an independently folded domain retaining its structure and F-actin binding property or is altered through interactions with the core. The flexibility and length of the core-to-headpiece linker sequence are also a major focus of our study. Because D6 of villin is proposed to contain a Ca^{2+}-binding site, our study also targets the role of calcium in regulation of the D6-HP fragment.

We find that for the stability of the folded, monomeric form of D6-HP, calcium is required in millimolar concentrations. We demonstrate that the D6-HP fragment consists of two structured domains, D6 and HP, separated by an unfolded linker sequence. The D6-HP calcium binding site is clearly associated with D6, the sequence of which is ~50% identical with that of domain 6 of gelsolin (G6) that also binds calcium. In the context of D6, the headpiece retains its three-dimensional structure. The 40-residue linker sequence is likely the longest interdomain connector in villin or gelsolin, suggesting the role of the villin headpiece as an independently acting domain. Our data indicate that the secondary structure of D6-HP corresponds to that of gelsolin domain G6 and the isolated headpiece. Surprisingly, we find that D6-HP bundles F-actin in the presence of high levels of calcium, suggesting an F-actin binding site on D6.

MATERIALS AND METHODS

Construction of the pD6-HP Expression Vector. The D6-HP fragment was designed to include the 208 C-terminal residues of chicken villin, including core domain 6, the linker sequence, and the headpiece domain (Figure 1). The construct was cloned from full-length chicken villin cDNA (a gift of P. Matsudaira, Whitehead Institute/Massachusetts Institute of Technology, Cambridge, MA) into the pET-24a vector (Novagen) using standard protocols (*23*). To produce the pD6-HP plasmid, PCR was used to amplify the designed sequence with primers containing an NdeI site at the 5′ end and a HindIII site at the 3′ end of the TAG stop codon.

Protein Sample Preparation. D6-HP was overexpressed from the pD6-HP plasmid in *Escherichia coli* line BL21-(DE3) (Novagen). After growth at 37 °C in Luria broth to an OD_{600} of ~0.6, the cells were harvested by centrifugation at 5000*g* for 30 min, washed in 1 L of the M9T medium, reharvested, and transferred to ^{13}C- and ^{15}N-labeled M9T medium for expression (*24*). The cells were equilibrated in the labeled M9T medium for 1 h, induced with 0.8 mM isopropyl β-D-1-thiogalactopyranoside (IPTG), and harvested after 4 h by centrifugation at 5000*g* for 30 min. The following lysis and gel filtration steps were performed in A buffer [50 mM NaCl, 5 mM dithiothreitol (DTT), 0.01% NaN_3, 20 mM sodium phosphate buffer (pH 7.0)]. The cells were lysed in A buffer by sonication in the presence of DNAse I (1 μg/mL), DTT (50 mM), and lysozyme (50 μg/mL). Cell debris was removed by centrifugation at 200,000*g* for 40 min. The supernatant was applied to a Sephadex G50 column (2 cm × 100 cm) run in A buffer at a rate of 0.5 mL/min. The D6-HP-containing fractions were combined and loaded onto HiTrap SP HP and HiTrap Q HP (GE Healthcare) columns (1 mL) connected to each other and equilibrated in 50 mM piperazine-1,4-bis(2-ethanesulfonic acid) (PIPES) (pH 7.0), 50 mM NaCl, and 5 mM $CaCl_2$. The flow-through that contained D6-HP protein free of DNA was collected at a flow rate of 1 mL/min and analyzed using SDS−PAGE which revealed a protein purity of >95%. Finally, the sample was concentrated and PIPES buffer replaced with d_{18}-PIPES with a 10 kDa molecular mass cutoff Amicon Ultra-4 concentrator (Millipore). Protein concentrations were determined by UV absorbance at 280 nm (*25*). The polypeptide identity was confirmed by mass spectrometry (Molecular Biology Core Facility, Dana Farber Cancer Institute, Boston, MA).

F-Actin Bundling by D6-HP. Actin was purified from chicken pectoral muscle using standard procedures (*26*) and was first incubated in F buffer [10 mM Tris (pH 8.0), 1 mM $MgCl_2$, 100 mM NaCl, 0.1 mM ATP, 0.2 mM DTT, 3 mM NaN_3, and 0.1 mM $CaCl_2$] overnight to allow polymerization. Purified D6-HP, 1.1 mM in 5 mM Ca^{2+}, was used as the source of D6-HP for the bundling assay. This D6-HP stock solution was diluted ~220-fold to yield a final concentration

of 5 μM and was incubated with F-actin at 2:1, 1:1, and 1:2 molar ratios in F buffer, either with or without the addition of 5 mM $CaCl_2$, for 45 min at 4 °C. Control F-actin and the F-actin/D6-HP mixtures were loaded on a carbon-coated and glow-discharged copper grid (SPI Supplies) for 1 min, washed with 10 drops of buffer containing 5 mM Tris and 50 mM sodium chloride (pH 7.5), and then stained with 1% uranyl acetate (*27*). All samples were imaged on a Philips CM12 transmission electron microscope operating at 120 kV with a LaB_6 filament and recorded on SO-163 EM (Kodak) film at a magnification of 45000× under minimal electron dose conditions. The film was processed with undiluted Kodak D-19 developer for 12 min and Kodak rapid fixer for 5 min. Electron micrographs were digitized on a Creo IQ Smart2 Scanner (Global Imaging) at 1270 dpi.

NMR Data Collection and Processing. The NMR samples consisted of 1.1 mM D6-HP, 10% ^2H_2O, 5 mM $CaCl_2$, 10 mM d_{10}-DTT, 0.01% NaN_3, and 20 mM d_{18}-PIPES (pH 7.0). The pH was adjusted with no correction for the effect of ^2H_2O. Two-dimensional (2D) and three-dimensional (3D) NMR data collection was performed at 25 °C on a Bruker AVANCE II 800 MHz spectrometer equipped with a Cryoprobe located at the Brandeis University NMR facility, and two spectrometers at Pacific Northwest National Laboratory's High Field Magnetic Resonance Facility, a Varian INOVA 750 MHz spectrometer with a room-temperature probe and a Varian Inova 600 MHz spectrometer outfitted with a cryoprobe. Processing of the NMR data was performed utilizing nmrPipe (*28*).

The ^{15}N HSQC spectrum of the isolated headpiece domain (HP67) was recorded at 25 °C on a Bruker DMX 500 MHz spectrometer at the Boston University Core Facility for Structural NMR. The assignment of the backbone ^1H and ^{15}N resonances of HP67 at 25 °C was performed by matching the cross-peaks to those published for an HP67 sample at 20 °C (BMRB entry 4428).

NMR Assignment. The backbone resonance (^1H, ^{15}N, and ^{13}C) assignment of the D6-HP sample was performed through a combined investigation of 2D ^{15}N HSQC (*29*, *30*) and the following 3D NMR data sets: HNCA (*31*), HN(CO)CA (*31*), HNCACB (*32*, *33*), CBCA(CO)NH (*34*), HNCO (*31*), HN(CA)CO (*35*), HNHA (*36*), HNHB (*37*), and HBHA(CO)NH (*38*). The side chain resonance (aliphatic ^1H and ^{13}C) assignments were obtained from HCCH-COSY (*39*), CC(CO)NH (*40*), and HC(CO)NH (*40*) NMR data. Aromatic side chain ^1H assignments were derived from dedicated heteronuclear 2D experiments (*41*). The visualization and analysis of the NMR spectra and the cross-peak picking were performed with NMRDRAW (*28*) and NMRVIEW (*42*). Chemical shifts for all nuclei are relative to the internal standard 3-(trimethylsilyl)tetradeuterosodium propionate (*43*).

NMR Relaxation Measurements and Order Parameter Computations. ^{15}N relaxation measurements were performed on a 750 MHz spectrometer using 2D proton-detected heteronuclear NMR experiments based on those of Farrow et al. (*51*). The R_1 relaxation rates were extracted from a series of spectra with relaxation delays of 100, 200, 300, 400, 600, 800, 1000, 1500, and 2000 ms. The R_2 rates were derived from experiments with relaxation delays of 10, 20, 30, 50, 70, 100, 130, 170, 210, and 250 ms. The heteronuclear $\{^1H-^{15}N\}$ NOE experiments were conducted with a proton saturation time of 2.5 s (NOEpresat) and without the presaturation (NOEnopresat). The $\{^1H-^{15}N\}$ NOE values were calculated as the $NOE_{presat}/NOE_{nopresat}$ ratio.

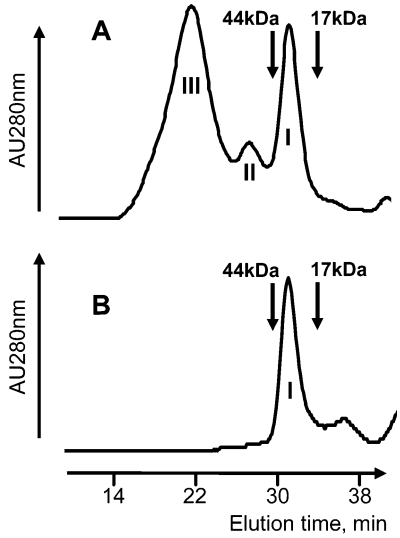

FIGURE 2: Ca^{2+} dependence of the aggregation state of D6-HP. (A) D6-HP in gel filtration buffer and (B) D6-HP in gel filtration buffer and 5 mM Ca^{2+}. I is the elution peak of monomeric D6-HP. II and III are elution peaks of D6-HP aggregates. Arrows indicate the positions of 44 and 17 kDa molecular mass standards, run separately (Bio-Rad). One hundred microliters of 1.5 mM D6-HP was run in a Superdex GL-200 column (Amersham) in gel filtration buffer [10 mM Tris, 150 mM NaCl, and 5 mM DTT (pH 7.5)] with a flow rate of 0.5 mL/min at 4 °C.

The R_1, R_2, and $\{^1H-^{15}N\}$ NOE values were determined by fitting the data intensities to exponentials using the routines in NMRVIEW (*42*). The Lipari−Szabo model-free order parameter S^2 (*44*) was calculated with FAST-Modelfree (*45*), a user-friendly interface to Modelfree (*46*, *47*). Of the total of 176 assigned ^{15}N HSQC backbone cross-peaks, 144 were included in the relaxation and $\{^1H-^{15}N\}$ NOE analysis. The 32 remaining resonances were excluded due to their low intensities or significant overlap with other cross-peaks.

Secondary Structure Element Detection. The secondary structure content of the D6-HP fragment was predicted by TALOS (*48*) on the basis of the backbone $^1H_\alpha$, ^{15}N, $^{13}C_\alpha$, and ^{13}CO and side chain $^{13}C_\beta$ chemical shift values. The standard TALOS reference protein set of 3D structures and resonances was used. This set did not include the isolated headpiece domain HP67 (*16*) or gelsolin-like domains.

RESULTS

Calcium Is Required for the Stability and Folding of the Monomeric Form of D6-HP. As described in Materials and Methods, the D6-HP polypeptide was labeled with ^{15}N and ^{13}C isotopes by expression in bacteria. The purification of the protein sample included gel filtration and ion exchange chromatography steps. Preliminary NMR data and gel filtration chromatography showed that D6-HP aggregates within hours (Figure 2A). The protein elutes in two major peaks (I and III) and one minor peak (II). The elution volume of peak I was consistent with a monomeric species, whereas peaks II and III indicated D6-HP oligomers. In NMR ^{15}N HSQC spectra (not shown), there were fewer resonances than we expected and many broad peaks at random coil chemical shifts, a pattern indicating a significant fraction of unfolded structure and/or protein aggregation. Notably, the set of cross-

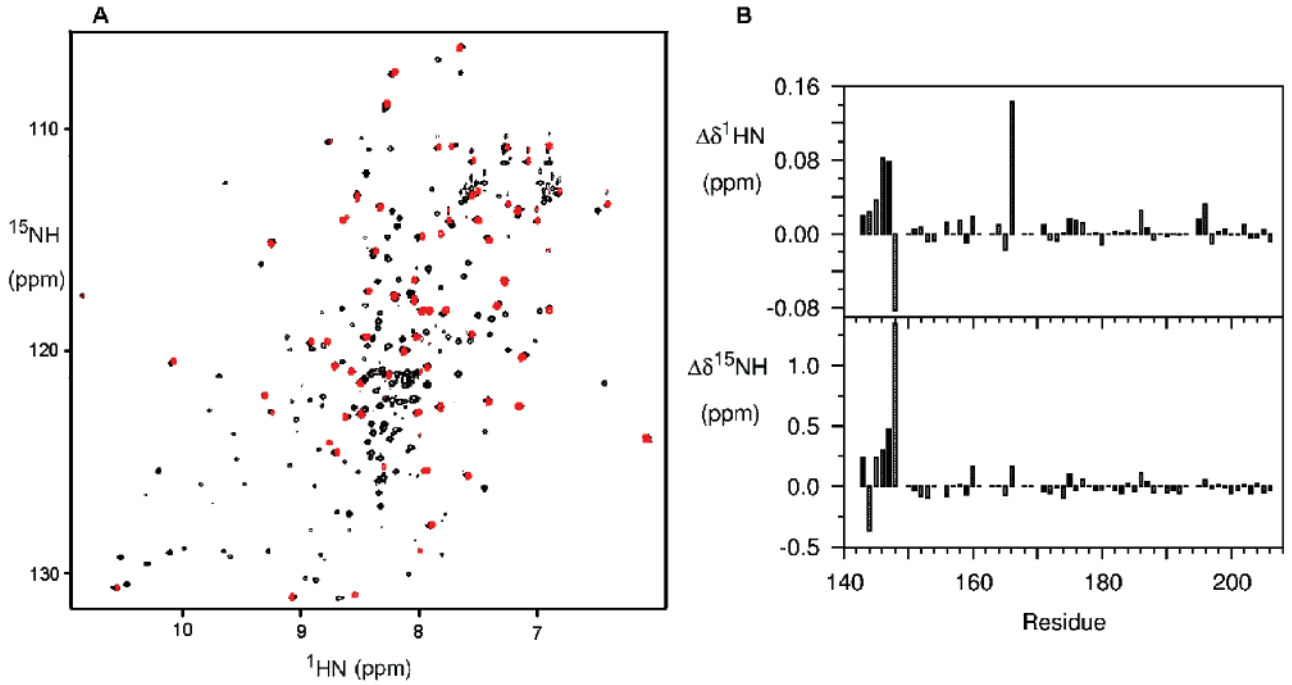

FIGURE 3: NMR characterization of D6-HP and comparison with the isolated headpiece (HP67). (A) ^{15}N HSQC spectra of D6-HP in 5 mM Ca^{2+} acquired at 800 MHz (black) and isolated headpiece, HP67, acquired at 500 MHz (red), both at 25 °C and pH 7.0. (B) Profile of the backbone ^{1}HN and ^{15}N chemical shift differences in the headpiece sequence between D6-HP and HP67 samples at 25 °C and pH 7.0.

peaks characteristic of the isolated headpiece domain (HP67) was clearly present. Alterations of temperature, pH, and NaCl level did not prevent the aggregation. However, the long-term stability of the monomeric form of D6-HP was achieved by inclusion of calcium at concentrations greater than 1 mM (Figure 2B). Therefore, we collected all the NMR data for D6-HP protein in the presence of 5 mM Ca^{2+}.

The ^{15}N HSQC spectrum of 1.1 mM D6-HP recorded at 25 °C and pH 7.0 in 5 mM Ca^{2+} (Figure 3A) indicates a folded, monomeric protein sample. The cross-peaks are sharp, and their number corresponds to that expected from the amino acid composition of the D6-HP sequence. The effect of calcium concentration on the spectra was sampled from 5 to 50 mM. There were no changes in the observed ^{15}N HSQC spectra. This suggests saturation of all available Ca^{2+} binding sites in D6-HP by 5 mM calcium.

The Headpiece Domain Retains Its Three-Dimensional Structure in D6-HP. We utilized the heteronuclear 3D NMR data recorded with a ^{13}C- and ^{15}N-labeled D6-HP sample to assign the backbone resonances (^{1}HN, ^{15}N, $^{13}C_{\alpha}$, and ^{13}CO) for 176 residues of the 208 in D6-HP using established procedures (*49*). Utilizing side chain-sensitive 3D NMR experiments, the side chain resonances were identified for 191 residues (92% of the sequence), including some of those without backbone assignments. Of the 17 residues for which no assignments are available, six are positioned on the extreme N- or C-terminus of the sequence. All other 11 unassigned residues are located between positions 60 and 85 (Figure 5). Of these 11 residues, three are prolines. The five-residue sequence (68−72) constitutes the longest continuous stretch of unassigned residues, suggesting a loop undergoing intermediate exchange. All the stretches of unassigned amino acids are flanked by residues whose ^{15}N HSQC signals are weak or missing, suggesting those regions are in intermediate structural exchange on the NMR time scale.

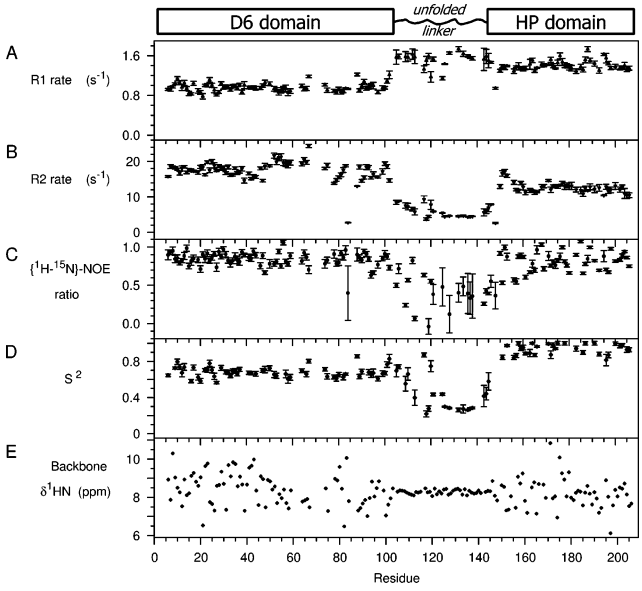

FIGURE 4: Relaxation rates, {^{1}H−^{15}N} NOE ratios, order parameters, and backbone ^{1}HN chemical shift values for D6-HP: (A) R_1, (B) R_2, (C) {^{1}H−^{15}N} NOE ratio, (D) Lipari−Szabo model-free order parameter, S^2, computed with FAST-Modelfree (*45*), and (E) backbone ^{1}HN chemical shift values. The domain structure of D6-HP derived from the presented data is displayed at the top.

The ^{15}N HSQC pattern of the isolated headpiece domain (*16*) corresponds well with the ^{15}N HSQC spectrum of D6-HP (Figure 3A). Each HP67 cross-peak directly overlaps with, or is positioned very closely to, the corresponding D6-HP resonance. Most of the ^{1}HN and ^{15}NH chemical shift differences (Figure 3B) are negligible (<0.04 ppm for ^{1}HN and <0.2 ppm for ^{15}NH), indicating very similar structural environments for the headpiece domain in D6-HP and HP67. The six N-terminal residues of HP67 display noticeable differences in chemical shift which can be attributed to the effect of the linker sequence of D6-HP influencing the

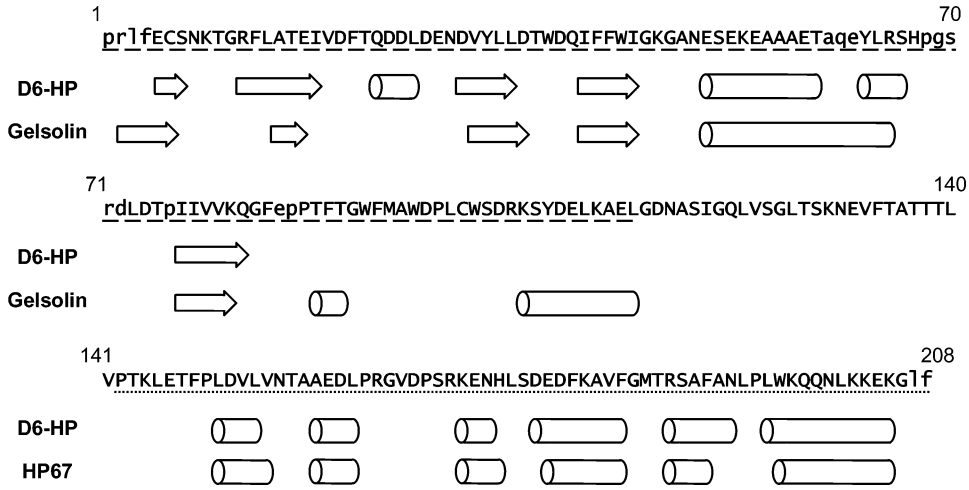

FIGURE 5: Comparison of the secondary structure of gelsolin, HP67, and D6-HP. The D6-HP sequence is underlined as follows: 50% identical to the gelsolin G6 domain (dashed underline), linker sequence (no underline), and villin headpiece (dotted underline). Secondary structure elements (cylinders represent helices and arrows β-sheets) of D6-HP, as predicted by TALOS (*48*), are mapped onto the D6-HP sequence. Secondary structure elements found in the crystal structures of the calcium-free gelsolin G6 domain and the isolated villin headpiece, HP67, are labeled Gelsolin and HP67, respectively. Residues in D6-HP for which no resonance assignments are available are denoted in lowercase.

N-terminal residues of the HP domain. One residue in the middle of the headpiece sequence, D166, displays a significantly higher than average ^{1}HN chemical shift difference (0.15 ppm) between D6-HP and HP67 samples (Figure 3B).

D6-HP Consists of Two Structured Domains, D6 and HP, Separated by an Unfolded Linker Sequence. The ^{15}N backbone relaxation rates R_1 and R_2 as well as the $\{^1$H$-^{15}$N$\}$ NOE (Figure 4A−C) indicate three distinct structural entities within D6-HP, namely, two structured regions, positions 1−105 and 145−206, and a disordered sequence between them. The order parameters (S^2) from the Lipari−Szabo model-free analysis (*44*) (Figure 4D) follow the same trend.

In agreement with the NMR relaxation data, the backbone ^{1}HN chemical shift profile (Figure 4E) indicates two regions, residues 1−105 and 145−206, with well-dispersed values indicative of a folded polypeptide. The linker sequence, positions 105−145, is characterized by the ^{1}HN chemical shift values narrowly clustered between 8.0 and 8.5 ppm consistent with a random coil, unfolded polypeptide. The $^1H_\alpha$ chemical shift profile has a similar pattern (not shown).

The ^{15}N HSQC spectrum (Figure 3A) clearly shows an uneven distribution of the intensities of the D6-HP cross-peaks. The strongest cross-peaks belong to residues in the D6-to-HP linker (residues 104−144); the weakest are from D6, and those from the HP domain are of intermediate intensity. This observation is consistent with the relative R2 relaxation rates (Figure 4B). The linker residues are nearly unrestrained, resulting in slower R2 relaxation rates and hence their higher ^{15}N HSQC intensity. On the other hand, the residues of the largest domain, D6, relax the fastest, and thus, their HSQC cross-peaks are the weakest. The resonances of the HP domain, which is structured but significantly smaller than D6, display intermediate HSQC peak intensities.

The large error bars in the $\{^1$H$-^{15}$N$\}$ NOE plot in the area of the linker are due to the generally low intensities of the NOE cross-peaks for these residues, which may be attributable to exchange of the backbone amides with water. Residue Phe84, in D6, stands out due to its low R_2 and low $\{^1$H$-^{15}$N$\}$ NOE ratio value (Figure 4B,C). Additionally, the Lipari−Szabo model-free analysis marked Phe84 as "unassigned". It should be noted here that the NMR resonances of the residue following Phe84 remain unassigned, possibly due to the intermediate exchange of this region of the sequence.

The D6-HP Secondary Structure Corresponds to That of Gelsolin Domain 6 and the Isolated Headpiece. Protein chemical shift values, especially $^1H_\alpha$, ^{15}NH, $^{13}C_\alpha$, ^{13}CO, and $^{13}C_\beta$, are good indicators of the secondary structure patterns. We employed TALOS (*48*) to predict the secondary structure elements in D6-HP using our chemical shift assignments. The secondary structure of D6-HP corresponds closely to that of domain 6 (G6) in the crystal structures of calcium-bound (*22*) or calcium-free gelsolin (*21*) and the isolated villin headpiece, HP67 (*17*) (Figure 5). The only major exception is the C-terminal helix of calcium-free gelsolin, which does not have a homologous counterpart in Ca^{2+}-bound D6-HP. The C-terminal helix of gelsolin is not visible in the calcium-bound crystal structure (*22*).

Calcium Binds to D6. The ^{15}N HSQC spectrum of D6-HP in the absence of calcium was compared to that in the presence of 5 mM calcium. Ninety-six D6-HP backbone amide resonances in a calcium-free HSQC spectrum were reliably assigned by comparison with the HSQC spectrum recorded in 5 mM calcium. They include 33 ^{1}HN resonances in the D6 sequence, 27 in the linker, and 36 in the HP domain. Without calcium, one-quarter of all the D6 backbone amide resonances either disappear or undergo significant changes in their chemical shift values. The presence of calcium affects the first 80 residues of D6, suggesting that calcium binding is important for the folding of this entire region. The remaining C-terminal part of D6 (positions 81−105), linker region, and HP domain are insensitive to calcium.

These data indicate that in the absence of calcium the headpiece domain remains structurally independent of D6 . All the most prominent changes in the D6-HP three-dimensional structure caused by the lack of calcium are associated with D6, not the headpiece or the linker region.

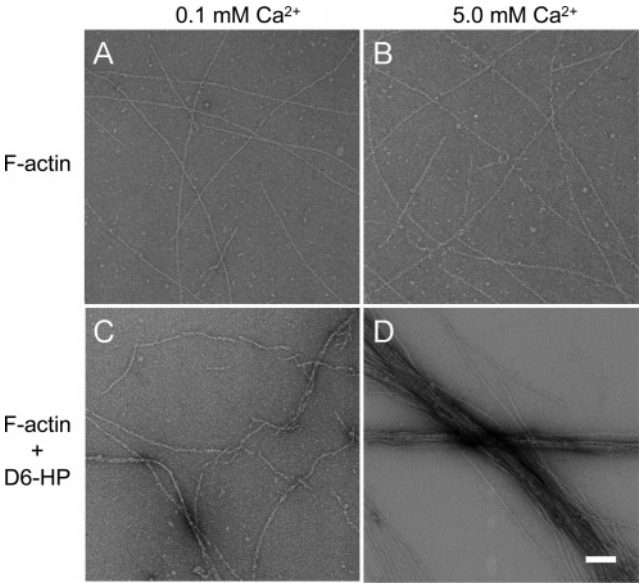

FIGURE 6: Negative stain electron micrographs of calcium-sensitive F-actin bundling by D6-HP. (A) F-Actin filaments (1 μM) in the presence of 0.1 mM calcium. (B) F-Actin filaments (1 μM) in the presence of 5 mM calcium. (C) F-Actin filaments with D6-HP in 0.1 mM calcium. (D) F-Actin bundles with D6-HP in 5 mM calcium. D6-HP and F-actin were both at 5 μM in experiments C and D. Samples were incubated at 4 °C for 45 min and negatively stained with 1% uranyl acetate. Images were recorded by transmission electron microscopy at a magnification of 45000×. The magnification bar (in panel D) is 100 nm for all the images.

D6-HP Bundles F-Actin in a Calcium-Sensitive Fashion. Villin is an F-actin bundling protein. Previous work (*2*) indicated that the N-terminal half of villin (core domains 1−3) and the headpiece represent the two F-actin binding sites required for F-actin bundling by villin. We confirmed that the D6-HP construct was still active with respect to actin binding using F-actin sedimentation assays (not shown). We also examined F-actin filaments decorated with D6-HP by negative stain electron microscopy. Surprisingly, we found that D6-HP organizes F-actin into bundles (Figure 6). We tested F-actin bundling by the D6-HP villin fragment at two levels of calcium (5 and 0.1 mM) and at D6-HP:G-actin molar ratios of 1:2, 1:1, and 2:1. In all the experiments, the incubation time was 45 min, significantly shorter than the time required for D6-HP aggregation at submillimolar calcium concentrations. This way, we ensured that any absence of F-actin bundling by D6-HP is not due to the aggregation of D6-HP. At 5 mM calcium, D6-HP bundles F-actin at any D6-HP:G-actin molar ratio (Figure 6D). Without D6-HP, no F-actin bundling was observed at either level of calcium (Figure 6A,B). D6-HP cannot bundle F-actin at a low calcium concentration (0.1 mM) (Figure 6C). This suggests that the Ca^{2+}-induced conformational change is essential for the cryptic F-actin binding site in D6-HP and further suggests that this actin binding site is in the D6 portion of the construct.

DISCUSSION

Villin Headpiece in the Context of the Core Domains. Our study of D6-HP is the first structural and dynamic characterization of a modular fragment of villin containing both a region of the core and the C-terminal headpiece domain. We envisioned two possible regimes for the villin headpiece: one in which it is tethered to the core by a flexible linker sequence and functions in a manner independent of the adjacent core domain and the other in which the headpiece and domain 6 of the core engage in strong steric interactions.

The results of our study clearly demonstrate that the headpiece retains its structure and is connected to the adjacent core D6 domain by a long, unstructured linker sequence. Therefore, the wealth of previous data (*11*, *16*) describing the properties and mode of interaction of the headpiece with F-actin applies to the headpiece in the context of attachment to the core domain. In addition to this fundamental result, our study highlights several surprising findings and poses new questions discussed below.

D6-HP Bundles F-Actin by Utilizing a Cryptic F-Actin Binding Site on D6. Villin is a modular protein which consists of the N-terminal gelsolin-like six-domain core and the C-terminal headpiece domain. Villin is a multifunctional actin accessory protein, the activity of which is regulated by several environmental messengers, including calcium. At physiological levels of calcium, villin bundles actin, whereas at higher calcium levels, villin can, like gelsolin, sever and cap actin filaments. Villin bundles F-actin by utilizing two F-actin binding sites, one in the C-terminal headpiece domain and the other at the N-terminus of the gelsolin-like core of villin (*2*, *11*). The isolated headpiece is capable of calcium-independent F-acting binding (*11*) and does not bundle filaments with or without calcium (See Supporting Information).

Surprisingly, we find that the D6-HP fragment is capable of bundling F-actin in the presence of 5 mM calcium (Figure 6). Domains 2 and 3 have been shown to be the F-actin binding site in the core domain of villin (*11*). Because in D6-HP the headpiece retains its "isolated" fold, is structurally independent of D6, and has only one F-actin binding site, we propose that villin core domain D6 has a cryptic, calcium-dependent F-actin binding site that is revealed when the domain is excised from the rest of the gelsolin-like core.

The Fold and Calcium Binding of D6 Resemble Those of Gelsolin Domain G6. The high degree of sequence identity between villin and gelsolin and the secondary structure similarity between D6 and gelsolin core domain 6 (G6) (Figure 5) suggest that the fold of D6 will likely be very similar to that of G6. Thus, we propose that villin D6 folds as a five-stranded β-sheet sandwiched between the long α-helix and a shorter helical region in the C-terminal sequence of the domain. This fold is typical for the gelsolin-like core domains whose structures are known (*15*, *22*, *50*).

Our data indicate that, in the absence of calcium, the first ~80 residues of D6-HP change their fold or are destabilized as compared to the D6-HP structure at a high calcium concentration. Without sufficient calcium in solution, D6-HP cannot bundle F-actin (Figure 6) and aggregates over the course of several hours. This suggests that calcium binding may play a vital role in regulating villin through a binding site located within the first 80 residues of D6. The location of this calcium binding site on D6 is different from the two sites on the surface of domain 1 of villin (14T), which were predicted to reside around residues 92 and 121, respectively (*14*).

On the basis of the sequence and secondary structure similarity to gelsolin domain G6, we propose villin residues Asn647, Asp648, and Glu670 (D6-HP residues Asn29,

Asp30, and Glu52, respectively) as the likely calcium binding site on the surface of D6 of villin. Two of these residues, Asp648 and Glu670, bind calcium via their side chains in the calcium-bound gelsolin structure (*22*) and are absolutely conserved in villin and gelsolin sequences. The third residue, Asn647, lends its backbone carbonyl oxygen to bind calcium, and this position varies between villin and gelsolin and among different species.

Unstructured Regions of D6. The chemical shift, R_1, R_2, and $\{^1H-^{15}N\}$ NOE data (Figure 4) indicate two structured domains in the D6-HP sequence, D6 and HP. Nevertheless, the NMR relaxation and assignment data suggest that some D6 residues are unstructured.

Seventeen residues in the D6-HP sequence remain unassigned (Figure 5). Four of them are positioned at the N-terminus and two at the C-terminus. All internal unassigned residues are located within the residues 60−85 of D6. The longest unassigned stretch in D6 includes five residues from Pro68 to Asp72. Because this region corresponds to the solvent-exposed loop in the crystal structure of the G6 domain of gelsolin (*22*), we propose that these residues are involved in intermediate structural exchange which weakens their NMR resonances. The second longest stretch of unassigned residues, Ala60-Gln61-Glu62, corresponds to an internal region of the longest helix of G6 in the gelsolin crystal structures. Why these D6-HP residues could not be assigned remains unclear.

Residue Phe84 in D6 appears to be unstructured as manifested by its low R_2 value (Figure 4C) and the $\{^1H-^{15}N\}$ NOE ratio of well below 0.6 (Figure 4C). In fact, the next residue, Glu85, is unassigned because the residue appears to be involved in structural exchange. In the gelsolin crystal structure, Phe84 and Glu85 correspond to a short unstructured loop on the solvent-exposed surface. Notably, the Phe84 residue is positioned close to the border between the Ca^{2+}-sensitive and Ca^{2+}-insensitive parts of D6.

The Core-to-Headpiece Linker Sequence Is the Longest Interdomain Region in Villin. Our data indicate that the unstructured linker sequence connecting structured D6 and HP consist of approximately 40 residues (positions 105−145) which are exposed to solvent (Figure 4). This core-to-headpiece linker sequence is likely the longest villin interdomain connector because it is significantly longer than any interdomain region in the gelsolin core (all fewer than 20 residues). Sequence alignments (not shown) indicate that the length of the villin core-to-HP linker sequence varies by only a few residues among species. The level of sequence identity in the villin core-to-headpiece linker region is ∼15%, significantly lower than in the D6 and HP domains where the level of sequence identity is ∼50%. Therefore, we conclude that the sequence connecting the gelsolin-like core of villin and the headpiece domain acts purely as an unstructured tether and is unlikely to be a recognition target for specific protein−protein interactions. These properties of the core-to-headpiece linker region of villin correlate well with the proposed role of the villin headpiece as a domain structurally independent from the gelsolin-like core and crucial for the functionality of villin.

The Headpiece Retains Its Structure. Our assignments of the NMR chemical shift values in the headpiece region of D6-HP are very close to those reported for the isolated headpiece, HP67. With the exception of several N-terminal residues of the HP67 sequence close to the linker sequence, most of the headpiece ^1H resonances in D6-HP differ from those in HP67 by less than 0.02 ppm. One D6-HP headpiece residue, D166, displays a significant difference (0.15 ppm) from the corresponding ^1H value for the isolated headpiece. This difference cannot be attributed to calcium, because the D166 backbone amide resonates at the same chemical shift in the presence and absence of calcium ions (not shown). Therefore, we expect to observe a slight structural alteration in the area of this residue in D6-HP as compared to the solution structure of the isolated headpiece.

CONCLUSIONS

Our study poses a number of new questions. The most important of them is why the core-to-headpiece linker in villin is so long. Stretched out completely, the 40-residue linker spans ∼120 Å, greater than the long axis of the folded calcium-free gelsolin (∼100 Å). Is the linker designed to allow the headpiece to interact with other core domains of villin? Does the long linker allow for more efficient F-actin bundling by villin? Is the interaction of the villin headpiece domain with the core calcium-sensitive? Future NMR studies and structural simulations of the complete villin under varying conditions will help to clarify this issue.

Our investigation highlights the role of calcium in structural and functional regulation of villin core domain 6 linked to the headpiece. The work presented here prepares the ground for the determination of the solution structure of D6-HP protein and for study of site-specific effects of calcium on the structure of this modular fragment of villin. Such an investigation will provide valuable insights into the functional and structural regulation of villin, a modular, calcium-sensitive, multipurpose F-actin regulating protein.

ACKNOWLEDGMENT

We acknowledge Mehul Dalal for construction of the pD6-HP expression vector and Jeffrey W. Brown for providing actin. We thank Olga Platonova for help in optimizing the purification procedure of the D6-HP sample. Elizabeth Luna provided valuable and greatly appreciated discussion of this work. We are grateful to Donna Baldisseri of Bruker Biospin Inc. (Billerica, MA) for the generous help in collecting preliminary NMR data. The assistance of Susan Pochapsky was instrumental in the collection of NMR spectra at the NIH-initiated regional NMR Center at Brandeis University. A portion of the research described in this paper was performed in the High Field Magnetic Resonance Facility of the Environmental Molecular Sciences Laboratory, a national scientific user facility sponsored by the Department of Energy's Office of Biological and Environmental Research and located at Pacific Northwest National Laboratory.

SUPPORTING INFORMATION AVAILABLE

The Supporting Information contains electron micrographs that demonstrate that the isolated villin headpiece does not bundle F-actin filaments. This material is available free of charge via the Internet at http://pubs.acs.org.

REFERENCES

1. Bretscher, A., and Weber, K. (1980) Villin is a major protein of the microvillus cytoskeleton which binds both G and F actin in a calcium-dependent manner, *Cell 20*, 839−847.

2. Friederich, E., Vancompernolle, K., Louvard, D., and Vandekerckhove, J. (1999) Villin function in the organization of the actin cytoskeleton. Correlation of in vivo effects to its biochemical activities in vitro, *J. Biol. Chem. 274*, 26751−26760.
3. Ferrary, E., Cohen-Tannoudji, M., Pehau-Arnaudet, G., Lapillonne, A., Athman, R., Ruiz, T., Boulouha, L., El Marjou, F., Doye, A., Fontaine, J. J., Antony, C., Babinet, C., Louvard, D., Jaisser, F., and Robine, S. (1999) In vivo, villin is required for Ca^{2+}-dependent F-actin disruption in intestinal brush borders, *J. Cell Biol. 146*, 819−830.
4. Glenney, J. R., Jr., and Weber, K. (1981) Calcium control of microfilaments: Uncoupling of the F-actin-severing and -bundling activity of villin by limited proteolysis in vitro, *Proc. Natl. Acad. Sci. U.S.A. 78*, 2810−2814.
5. Kwiatkowski, D. J., Stossel, T. P., Orkin, S. H., Mole, J. E., Colten, H. R., and Yin, H. L. (1986) Plasma and cytoplasmic gelsolins are encoded by a single gene and contain a duplicated actin-binding domain, *Nature 323*, 455−458.
6. Bazari, W. L., Matsudaira, P., Wallek, M., Smeal, T., Jakes, R., and Ahmed, Y. (1988) Villin sequence and peptide map identify six homologous domains, *Proc. Natl. Acad. Sci. U.S.A. 85*, 4986−4990.
7. Matsudaira, P., and Janmey, P. (1988) Pieces in the actin-severing protein puzzle, *Cell 54*, 139−140.
8. Mahajan-Miklos, S., and Cooley, L. (1994) The villin-like protein encoded by the *Drosophila* quail gene is required for actin bundle assembly during oogenesis, *Cell 78*, 291−301.
9. Pestonjamasp, K. N., Pope, R. K., Wulfkuhle, J. D., and Luna, E. J. (1997) Supervillin (p205): A novel membrane-associated, F-actin-binding protein in the villin/gelsolin superfamily, *J. Cell Biol. 139*, 1255−1269.
10. Rana, A. P., Ruff, P., Maalouf, G. J., Speicher, D. W., and Chishti, A. H. (1993) Cloning of human erythroid dematin reveals another member of the villin family, *Proc. Natl. Acad. Sci. U.S.A. 90*, 6651−6655.
11. Pope, B., Way, M., Matsudaira, P. T., and Weeds, A. (1994) Characterisation of the F-actin binding domains of villin: Classification of F-actin binding proteins into two groups according to their binding sites on actin, *FEBS Lett. 338*, 58−62.
12. Azim, A. C., Knoll, J. H., Beggs, A. H., and Chishti, A. H. (1995) Isoform cloning, actin binding, and chromosomal localization of human erythroid dematin, a member of the villin superfamily, *J. Biol. Chem. 270*, 17407−17413.
13. Finidori, J., Friederich, E., Kwiatkowski, D. J., and Louvard, D. (1992) In vivo analysis of functional domains from villin and gelsolin, *J. Cell Biol. 116*, 1145−1155.
14. Markus, M. A., Nakayama, T., Matsudaira, P., and Wagner, G. (1994) Solution structure of villin 14T, a domain conserved among actin-severing proteins, *Protein Sci. 3*, 70−81.
15. Markus, M. A., Matsudaira, P., and Wagner, G. (1997) Refined structure of villin 14T and a detailed comparison with other actin-severing domains, *Protein Sci. 6*, 1197−1209.
16. Vardar, D., Buckley, D. A., Frank, B. S., and McKnight, C. J. (1999) NMR structure of an F-actin-binding "headpiece" motif from villin, *J. Mol. Biol. 294*, 1299−1310.
17. Meng, J., Vardar, D., Wang, Y., Guo, H. C., Head, J. F., and McKnight, C. J. (2005) High-resolution crystal structures of villin headpiece and mutants with reduced F-actin binding activity, *Biochemistry 44*, 11963−11973.
18. Vermeulen, W., Vanhaesebrouck, P., Van Troys, M., Verschueren, M., Fant, F., Goethals, M., Ampe, C., Martins, J. C., and Borremans, F. A. (2004) Solution structures of the C-terminal headpiece subdomains of human villin and advillin, evaluation of headpiece F-actin-binding requirements, *Protein Sci. 13*, 1276−1287.
19. Kumar, N., and Khurana, S. (2004) Identification of a functional switch for actin severing by cytoskeletal proteins, *J. Biol. Chem. 279*, 24915−24918.
20. Janmey, P. A., and Matsudaira, P. T. (1988) Functional comparison of villin and gelsolin. Effects of Ca^{2+}, KCl, and polyphosphoinositides, *J. Biol. Chem. 263*, 16738−16743.
21. Burtnick, L. D., Koepf, E. K., Grimes, J., Jones, E. Y., Stuart, D. I., McLaughlin, P. J., and Robinson, R. C. (1997) The crystal structure of plasma gelsolin: Implications for actin severing, capping, and nucleation, *Cell 90*, 661−670.
22. Kolappan, S., Gooch, J. T., Weeds, A. G., and McLaughlin, P. J. (2003) Gelsolin domains 4−6 in active, actin-free conformation identifies sites of regulatory calcium ions, *J. Mol. Biol. 329*, 85−92.
23. Sambrook, J., Fritsch, E. F., and Maniatis, T. (1989) *Molecular Cloning: A Laboratory Manual*, Cold Spring Harbor Laboratory Press, Plainview, NY.
24. Marley, J., Lu, M., and Bracken, C. (2001) A method for efficient isotopic labeling of recombinant proteins, *J. Biomol. NMR 20*, 71−75.
25. Edelhoch, H. (1967) Spectroscopic determination of tryptophan and tyrosine in proteins, *Biochemistry 6*, 1948−1954.
26. Pardee, J. D., and Spudich, J. A. (1982) Purification of muscle actin, *Methods Enzymol. 85* (Part B), 164−181.
27. Harris, J. R., and Horne, R. W. (1991) Negative staining, in *Electron Microscopy in Biology*, pp 203−228, IRL Press, Oxford, U.K.
28. Delaglio, F., Grzesiek, S., Vuister, G. W., Zhu, G., Pfeifer, J., and Bax, A. (1995) NMRPipe: A multidimensional spectral processing system based on UNIX pipes, *J. Biomol. NMR 6*, 277−293.
29. Palmer, A. G., Cavanagh, J., Wright, P. E., and Rance, M. (1991) Sensitivity improvement in proton-detected two-dimensional heteronuclear correlation NMR spectroscopy, *J. Magn. Reson. 93*, 151−170.
30. Kay, L. E., Keifer, P., and Saarinen, T. (1992) Pure absorption gradient enhanced heteronuclear single quantum correlation spectroscopy with improved sensitivity, *J. Am. Chem. Soc. 114*, 10663−10665.
31. Grzesiek, S., and Bax, A. (1992) Improved 3D triple-resonance NMR techniques applied to a 31 kDa protein, *J. Magn. Reson. 96*, 432−440.
32. Wittekind, M., and Mueller, L. (1993) HNCACB, a High-Sensitivity 3D NMR Experiment to Correlate Amide-Proton and Nitrogen Resonances with the α- and β-Carbon Resonances in Proteins, *J. Magn. Reson., Ser. B 101*, 201−205.
33. Muhandiram, D. R., and Kay, L. E. (1994) Gradient-Enhanced Triple-Resonance Three-Dimensional NMR Experiments with Improved Sensitivity, *J. Magn. Reson., Ser. B 103*, 203−216.
34. Grzesiek, S., and Bax, A. (1992) Correlating backbone amide and side chain resonances in larger proteins by multiple relayed triple resonance NMR, *J. Am. Chem. Soc. 114*, 6291−6293.
35. Yamazaki, T., Lee, W., Arrowsmith, C. H., Muhandiram, D. R., and Kay, L. E. (1994) A Suite of Triple Resonance NMR Experiments for the Backbone Assignment of ^{15}N, ^{13}C, ^{2}H Labeled Proteins with High Sensitivity, *J. Am. Chem. Soc. 116* (26), 11655−11666.
36. Vuister, G. W., and Bax, A. (1993) Quantitative J correlation: A new approach for measuring homonuclear three-bond $J_{HNH\alpha}$ coupling constants in ^{15}N-enriched proteins, *J. Am. Chem. Soc. 115* (17), 7772−7777.
37. Archer, S. J., Ikura, M., Torchia, D. A., and Bax, A. (1991) An alternative 3D NMR technique for correlating backbone ^{15}N with side chain Hβ resonances in larger proteins, *J. Magn. Reson. 95*, 636−641.
38. Grzesiek, S., and Bax, A. (1993) Amino acid type determination in the sequential assignment procedure of uniformly $^{13}C/^{15}N$-enriched proteins, *J. Biomol. NMR 3*, 185−204.
39. Clore, G. M., Bax, A., Driscoll, P. C., Wingfield, P. T., and Gronenborn, A. M. (1990) Assignment of the side-chain ^{1}H and ^{13}C resonances of interleukin-1β using double- and triple-resonance heteronuclear three-dimensional NMR spectroscopy, *Biochemistry 29* (35), 8172−8184.
40. Grzesiek, S., Anglister, J., and Bax, A. (1993) Correlation of Backbone Amide and Aliphatic Side-Chain Resonances in $^{13}C/^{15}N$-Enriched Proteins by Isotropic Mixing of ^{13}C Magnetization, *J. Magn. Reson., Ser. B 101*, 114−119.
41. Yamazaki, T., Forman-Kay, J. D., and Kay, L. E. (1993) Two-Dimensional NMR Experiments for Correlating ^{13}CB and $^{1}Hd/e$ Chemical Shifts of Aromatic Residues in ^{13}C-Labeled Proteins via Scalar Couplings, *J. Am. Chem. Soc. 115*, 11054−11055.
42. Johnson, B. A., and Blevins, R. A. (1994) NMRView: A computer program for the visualization and analysis of NMR data, *J. Biomol. NMR 4*, 603−614.
43. Wishart, D. S., Bigam, C. G., Yao, J., Abildgaard, F., Dyson, H. J., Oldfield, E., Markley, J. L., and Sykes, B. D. (1995) ^{1}H, ^{13}C and ^{15}N chemical shift referencing in biomolecular NMR, *J. Biomol. NMR 6*, 135−140.
44. Lipari, G., and Szabo, A. (1980) Effect of librational motion on fluorescence depolarization and nuclear magnetic resonance relaxation in macromolecules and membranes, *Biophys. J. 30*, 489−506.

45. Cole, R., and Loria, J. P. (2003) FAST-Modelfree: A program for rapid automated analysis of solution NMR spin-relaxation data, *J. Biomol. NMR 26*, 203−213.
46. Mandel, A. M., Akke, M., and Palmer, A. G., III (1995) Backbone dynamics of *Escherichia coli* ribonuclease HI: Correlations with structure and function in an active enzyme, *J. Mol. Biol. 246*, 144−163.
47. Palmer, A. G., Rance, M., and Wright, P. E. (1991) Intramolecular motions of a zinc finger DNA-binding domain from Xfin characterized by proton-detected natural abundance ^{13}C heteronuclear NMR spectroscopy, *J. Am. Chem. Soc. 113*, 4371−4380.
48. Cornilescu, G., Delaglio, F., and Bax, A. (1999) Protein backbone angle restraints from searching a database for chemical shift and sequence homology, *J. Biomol. NMR 13*, 289−302.
49. Cavanagh, J., Fairbrother, W. J., Palmer, A. G., and Skelton, N. J. (1996) *Protein NMR Spectroscopy: Principles and Practice*, Academic Press, San Diego.
50. Schnuchel, A., Wiltscheck, R., Eichinger, L., Schleicher, M., and Holak, T. A. (1995) Structure of severin domain 2 in solution, *J. Mol. Biol. 247*, 21−27.
51. Farrow, N. A., Muhandiram, R., Singer, A. U., Pascal, S. M., Kay, C. M., Gish, G., Shoelson, S. E., Pawson, T., Forman-Kay, J. D., Kay, L. E. (1994) Backbone dynamics of a free and a phosphopeptide-complexed Src homology 2 domain studied by 15N NMR relaxation, *Biochemistry 33*, 5984−6003.

BI700110V